

Pathway of ATP Hydrolysis by Monomeric and Dimeric Kinesin<sup>†</sup>Michele L. Moyer, Susan P. Gilbert,<sup>‡</sup> and Kenneth A. Johnson\*

Department of Biochemistry and Molecular Biology, 106 Althouse Laboratory, Pennsylvania State University, University Park, Pennsylvania 16802

Received May 13, 1997; Revised Manuscript Received September 26, 1997

**ABSTRACT:** The ATPase mechanism for a monomeric *Drosophila* kinesin construct, K341, was determined by pre-steady-state kinetic methods and compared to dimeric kinesin, K401. We directly measured the kinetics of binding mantATP (a fluorescent ATP analog) to the microtubule•K341 complex, the dissociation of K341 from the microtubule, and release of phosphate and ADP from K341. Measurements of phosphate release kinetics at low salt concentration show that K341 hydrolyzes 18 molecules of ATP per kinesin monomer prior to release from the microtubule. At a higher salt concentration the amplitude of the pre-steady-state burst of phosphate release was reduced to 8 molecules per kinesin monomer. The maximum rate of dissociation of K341 from the microtubule following the addition of ATP was 22 s<sup>-1</sup>. The rate of mantADP release from the M•K341•mantADP complex increased as a function of tubulin concentration with a second-order rate constant of 11 μM<sup>-1</sup> s<sup>-1</sup> for K341 binding to the microtubule and reached a maximum rate of mantADP release of 303 s<sup>-1</sup>. ADP release kinetics were also determined by monitoring the binding of mantATP to K341•ADP and K401•ADP after mixing with microtubules. We show that monomeric kinesin remains associated with the microtubule through multiple rounds of ATP hydrolysis. This apparent processivity implies that one of the functions of the cooperative interaction between the two kinesin heads in dimeric kinesin is for the reactions occurring on one kinesin head to facilitate the release of the adjacent head from the microtubule.

Molecular<sup>1</sup> motors have the unique ability to convert the chemical energy of ATP hydrolysis into directional movement and are involved in a wide range of processes essential to life. Myosin generates motility along actin filaments and functions in muscle contraction, organelle movement, and cytokinesis. Kinesin produces movement to transport organelles toward the plus ends of microtubules, oriented toward the cell surface. Kinesin and myosin have several superficial characteristics in common. Both are composed of two light chains and two heavy chains (Bloom et al., 1988; Kuznetsov et al., 1988; Weeds & Lowey, 1971). The heavy chains of both enzymes dimerize to form two amino-terminal globular head domains which contain the ATP binding site and the binding site for their respective filamentous substrates (Yang et al., 1990; Lowey & Cohen, 1962). Kinesin and myosin have even been found to have similar ATPase sites (Rayment et al., 1993; Kull et al., 1996) suggesting that they have evolved from a common precursor and that they may have similar strategies for energy transduction, yet each is uniquely adapted to its specific function.

Motility assays based upon video-enhanced light microscopy have described the central features of movement such as the step size, translocation velocity, and force produced by kinesin. Kinesin movement has been described as processive in that a single dimeric kinesin molecule can translocate for several micrometers along the microtubule without dissociating (Howard et al., 1989; Block et al., 1990). The relatively long distance traveled by kinesin before detachment occurs implies that kinesin spends a majority of its mechanochemical cycle in contact with the microtubule, in marked contrast to actomyosin.

Truncation of the kinesin heavy chain to the N-terminal 340 amino acids produces a monomeric kinesin molecule containing the ATP and microtubule binding sites of the motor (Moyer et al., 1996; Correia et al., 1995; Huang & Hackney, 1994b; Lockhart et al., 1995; Ma & Taylor, 1997a). For kinesin, the maximum rate of ATP hydrolysis is significantly elevated for monomeric kinesin compared to that of dimeric kinesin while motility rates observed, at high surface density, are slower for monomeric kinesin (Vale et al., 1996; Berliner, Young, 1995; Stewart et al., 1993). There is no evidence to indicate that an individual single-headed kinesin molecule can support movement (Berliner et al., 1995; Vale et al., 1996) and the data presented in this report suggest that ATP hydrolysis by monomeric kinesin is uncoupled from force production.

Evidence of interaction between the two motor domains of kinesin has been suggested by *in vitro* motility assays and biochemical studies (Hackney, 1994a; Howard et al., 1989; Gilbert et al., 1995; Block et al., 1990; Ma & Taylor,

<sup>†</sup> This work is supported by grants to K.A.J. (GM 26726 from the National Institutes of Health) and to M.L.M. (training grant GM 08358 from the National Institutes of Health).

\* Author to whom correspondence should be addressed. Tel: (814) 865-1200. Fax: (814) 865-3030. E-mail: kaj1@psu.edu.

<sup>‡</sup> Present address: Department of Biological Sciences, 518 Langley Hall, University of Pittsburgh, Pittsburgh, PA 15260.

<sup>1</sup> Abbreviations: cordycepin 5'-triphosphate (3'-dATP), 2'-deoxyadenosine 5'-triphosphate (2'-dATP), 2'(3')-O-(N-methylanthraniloyl)-adenosine 5'-diphosphate (mantADP), 2'(3')-O-(N-methylanthraniloyl)-adenosine 5'-triphosphate (mantATP).

1997b; Jiang & Hackney, 1997; Jiang et al., 1997). Interactions between the heads of kinesin may make a significant contribution to the pathway of force production. In an effort to understand the interactions between the two heads of kinesin, we have studied the pre-steady-state kinetics of a monomeric kinesin, K341, using stopped-flow techniques.

## EXPERIMENTAL PROCEDURES

**Materials.** Taxol was obtained from CalBiochem (La Jolla, CA). Radiolabeled ATP ( $[\alpha^{32}\text{P}]$  ATP, >3000 Ci/mmol) was from ICN Biomedicals, Inc. (Costa Mesa, CA). Silica gel 60 F<sub>254</sub> TLC plates (EM Separations of E. Merck, 20 × 20 cm, plastic backed) were obtained from VWR Scientific (Pittsburgh, PA). DEAE Sepharose FF was from Pharmacia LKB (Uppsala, Sweden). Nucleotides (ATP, 2'-deoxyATP, and 3'-deoxyATP), purine nucleoside phosphorylase, and 7-methylguanosine were obtained from Sigma Chemical Co. (St. Louis, MO). Dansyl chloride and *N*-methylisatoic anhydride were purchased from Molecular Probes (Eugene, OR).

**Buffers.** The following buffers were used for the experiments described: ATPase buffer (50 mM HEPES, pH 7.2, 5 mM Magnesium acetate, 0.1 mM EDTA, 0.1 mM EGTA, 50 mM potassium acetate, and 1 mM DTT); PM buffer (100 mM Pipes, pH 6.7, 5 mM magnesium acetate, and 1 mM EGTA).

**Protein Purification.** Procedures for the expression and purification of monomeric (K341) and dimeric (K401) *Drosophila* kinesin constructs have been described previously (Gilbert & Johnson, 1993; Moyer et al., 1996). The protein concentration of K401 was determined spectrophotometrically using extinction coefficient 293 450 M<sup>-1</sup> cm<sup>-1</sup> for K401 containing one ADP bound per active site (Gilbert & Johnson, 1993). Previous evaluation of several preparations of K401 has shown the active site concentration (determined by stoichiometry of binding  $[\alpha^{32}\text{P}]$  ADP in a nitrocellulose binding assay) to be equal to K401 concentration on the basis of spectrophotometric protein determination (Gilbert & Johnson, 1993; Gilbert & Johnson, 1994). The active-site concentration of K341 was determined by the phosphocreatine kinase coupled enzyme assay (Moyer et al., 1996). Three preparations of K401 and two preparations of K341 were used in the experiments reported. Each preparation was evaluated by steady-state ATPase assay to determine  $k_{\text{cat}}$  in the presence of saturating concentrations of microtubules and ATP. Little variability was observed between kinesin preparations. For K401,  $k_{\text{cat}} = 20 \pm 2 \text{ s}^{-1}$ ,  $K_{\text{m,ATP}} = 61 \pm 8.4 \mu\text{M}$ , and  $K_{0.5,\text{MT}} = 0.9 \pm 0.3 \mu\text{M}$  for three different preparations. For K341,  $k_{\text{cat}} = 84 \pm 4 \text{ s}^{-1}$ ,  $K_{\text{m,ATP}} = 101 \pm 10 \mu\text{M}$ , and  $K_{0.5,\text{MT}} = 3.3 \pm 0.4 \mu\text{M}$  for two different preparations. The quaternary structures of K401 and K341 have been determined by sedimentation velocity and sedimentation equilibrium centrifugation (Correia et al., 1995). K401 has been shown to be dimeric with a  $K_d$  of dimerization of  $37 \pm 17 \text{ nM}$ . K341 has been shown to be monomeric at concentrations up to at least 10  $\mu\text{M}$  total protein.

Bovine brain microtubules were prepared by two cycles of temperature-dependent polymerization and depolymerization (Sloboda et al., 1976; Shelanski et al., 1973), and tubulin was separated from microtubule-associated protein

by the method of Borisy et al. (1974) as modified by Omoto and Johnson (1986). On the day of each experiment an aliquot of tubulin was thawed, diluted to 10–15 mg/mL protein with PM buffer, adjusted to 1 mM GTP, and cold-depolymerized for 30 min on ice. The tubulin was then centrifuged (microfuge, 14 000 rpm, 15 min, 4 °C) to sediment aggregates of tubulin. The supernatant was adjusted to 20  $\mu\text{M}$  taxol and incubated at 34 °C for 10 min to polymerize the microtubules. The microtubules were then diluted in PM buffer plus 20  $\mu\text{M}$  taxol to dilute the GTP concentration to 0.1 mM and stabilize the microtubules. The preparation was incubated for an additional 20 min at 34 °C followed by centrifugation (SS34 rotor, 18 000 rpm, 20 min, 25 °C). The microtubule pellet was resuspended in ATPase buffer plus 20  $\mu\text{M}$  taxol, and the protein concentration was determined by the Schacterie and Pollack (1973) modification of Lowry et al. (1951).

**Dansyl Chloride Labeling of Microtubules.** Microtubules were labeled 1:1 with dansyl chloride. The kinetics of K341 dissociation from the labeled microtubules were not changed by labeling at higher ratios of label to tubulin (data not shown).

Microtubules were prepared as described above with the final pellet resuspended in PM buffer plus 20  $\mu\text{M}$  taxol. After the protein concentration was determined, the microtubules were diluted to 100  $\mu\text{M}$  tubulin with PM buffer plus 20  $\mu\text{M}$  taxol. Dansyl chloride (at 10 mM in acetone) was then added to a final concentration of 100  $\mu\text{M}$ . The reaction mixture was diluted 1:5 with PM buffer plus 20  $\mu\text{M}$  taxol and mixed for 30 min at room temperature (final concentrations of tubulin and dansyl chloride of 20  $\mu\text{M}$ ). The reaction mixture was then centrifuged (SS34 rotor, 18 000 rpm, 20 min, 25 °C). The pellet was resuspended in 1 mL of PM buffer plus 20  $\mu\text{M}$  taxol to remove excess label and centrifuged again as above. The final pellet was resuspended in ATPase buffer plus 20  $\mu\text{M}$  taxol, and protein concentration of the dansyl chloride labeled microtubules was determined by the Schacterie and Pollack (1973) modification of Lowry et al. (1951).

**Steady-State ATPase Assays.** ATPase measurements were made by following the hydrolysis of  $[\alpha^{32}\text{P}]$ ATP to form product  $[\alpha^{32}\text{P}]$ ADP as described previously (Gilbert & Johnson, 1993). K341 at a concentration of 0.10  $\mu\text{M}$  was used in the steady-state assays. At this concentration of K341 the construct is monomeric (Correia et al., 1995). In the absence of microtubules, reaction times sampled were from 0 to 20 min. In the presence of microtubules, reaction times sampled were from 0 to 75 s. Steady-state assays with mantATP were performed by quantifying phosphate by the malachite green assay (Lanzetta et al., 1979). Concentrations reported in figure legends are final concentrations after mixing reactants. The data were fit to a hyperbola by nonlinear regression using Kaleidograph (Synergy Software, Reading, PA) to determine steady-state kinetic constants.

**Nucleotide Analogs.** The *N*-methylantraniloyl derivatives of adenine nucleotides (Hiratsuka, 1983) were synthesized and characterized essentially as described (Woodward et al., 1991). Analogs were purified by DEAE Sepharose FF chromatography. The column was eluted with a linear gradient from 20 to 800 mM triethylammonium bicarbonate. Purity of mantADP and mantATP was confirmed by TLC using silica gel 60, F<sub>254</sub> in 1-propanol/NH<sub>4</sub>OH/water 6:3:1, v/v, containing 0.5 g/L EDTA. The spectrophotometric

properties of all analogs were tested. The  $A_{256}/A_{357}$  ratio of 2'(3')-mantATP and 2'(3')-mantADP was approximately 4, indicating that a monosubstituted derivative was obtained (Moore & Lohman, 1994).

**Transient Kinetic Measurements.** Stopped-flow experiments were performed using a KinTek StopFlow System (Model SF-2001, KinTek Corp., State College, PA). Dead time of the instrument was 1.8–2.2 ms. All assays were performed at 25 °C in ATPase buffer with concentrations being final values after mixing. All traces shown represent the average of four–six stopped-flow traces. Within each series of experiments, the group of fluorescence transients was normalized relative to the transient showing the largest amplitude of reaction by subtracting the minimum value of fluorescence and dividing by the maximum:  $F_i = (F_{t,obs} - F_{min})/F_{max}$ . This same scaling factor was used for each transient within the series so that the relative change in fluorescence is given with respect to the largest change in fluorescence observed.

**Binding of mantATP to Kinesin.** Kinetics of mantATP binding were measured in the stopped-flow. An excitation wavelength of 280 nm was used in all experiments in which mantATP binding was studied. By using an excitation wavelength of 280 nm, the mant fluorophore was excited by way of energy transfer from tryptophan and/or tyrosine residues present in the kinesin proteins. Fluorescence emission was monitored using a 400 nm cutoff long-wave pass filter.

The rates of mantATP binding to kinesin•ADP and the M•K complex were studied. In the first experiment, kinesin (5  $\mu$ M with ADP bound at the active site) was rapidly mixed with microtubules (12  $\mu$ M tubulin) and increasing concentrations of mantATP. Binding of mantATP to the M•K complex was measured by rapidly mixing the complex (12  $\mu$ M tubulin plus 5  $\mu$ M kinesin) with increasing concentrations of mantATP. At a concentration of 5  $\mu$ M, K341 and K401 have been found to be monomeric and dimeric, respectively (Correia et al., 1995).

**Release of mantADP from K341.** Release of mantADP from K341 in the presence of microtubules was measured in the stopped-flow. An excitation wavelength of 360 nm was used to study mantADP release from K341. Fluorescence emission was monitored using a 400 nm cutoff long-wave pass filter. K341•mantADP was prepared by incubating K341 (with ADP bound at the active site) with mantADP at a ratio of 1:2 (kinesin:mantADP) at 25 °C for 20 min. K341•mantADP (2  $\mu$ M K341 preincubated with 4  $\mu$ M mantADP) was then rapidly mixed with increasing concentrations of microtubules plus 1 mM ATP. K341 at 2  $\mu$ M is monomeric (Correia et al., 1995).

**Dissociation of M•K341 Complex.** The rate constant of microtubule•K341 dissociation was measured in two different stopped-flow experiments. First, the change in turbidity was measured when the M•K341 complex (1.35  $\mu$ M tubulin plus 1.5  $\mu$ M K341) was rapidly mixed with increasing concentrations of ATP plus 100 mM KCl. Turbidity was monitored at 340 nm. At a total protein concentration of 1.5  $\mu$ M, K341 is monomeric (Correia et al., 1995). Second, the change in fluorescence was measured when the M•K341 complex in which the microtubules were dansyl chloride labeled (1.35  $\mu$ M tubulin labeled 1:1 with dansyl chloride plus 1.5  $\mu$ M K341) was rapidly mixed with increasing concentrations

of ATP plus 100 mM KCl. The change in fluorescence was measured using an excitation wavelength of 325 nm. Fluorescence emissions were monitored using a 450 nm cut off long-wave pass filter.

**Phosphate Release Kinetics.** Phosphate release kinetics were measured directly in the stopped-flow using a fluorescent coupled assay (Brune et al., 1994). The coupled assay system employed the A197C mutant of the *Escherichia coli* phosphate-binding protein (PBP) covalently modified at cysteine 197 by *N*-[2-(1-maleimidyl)ethyl]-7-(diethylamino)-coumarin-3-carboxamide (MDCC) to produce the fluorescent reporter molecule. Background phosphate was removed from the buffer and solutions by a “phosphate mop”. The “phosphate mop” consisted of 0.03 u/mL purine nucleoside phosphorylase plus 0.1 mM 7-methylguanosine. To convert relative fluorescence change (volts) to concentration of phosphate released ( $\mu$ M) preliminary experiments in which 2  $\mu$ M probe (MDCC-PBP) was rapidly mixed with excess  $\text{KH}_2\text{PO}_4$  were performed. The fluorescence change that occurred upon phosphate binding to MDCC-PBP (2  $\mu$ M) was measured as the M•K341 complex (0.075  $\mu$ M tubulin plus 0.05  $\mu$ M K341) was rapidly mixed with 500  $\mu$ M ATP in the presence and absence of 100 mM KCl. At a total protein concentration of 0.05  $\mu$ M, K341 is monomeric (Correia et al., 1995). An excitation wavelength of 425 nm was used. Fluorescence emissions were monitored using a 450 nm cutoff long-wave pass filter.

**Data Analysis.** Transient kinetic data were analyzed by conventional fitting methods and then by global analysis to a minimal mechanism based upon computer simulation. Conventional fitting methods involve fitting the time course to a function of one, two, or three exponentials alone or in combination with a linear phase. The concentration dependence of the observed rates is then used to deduce a mechanism, and fitting to a model is done by examination of the predicted concentration dependence of the rates based upon analytical solution of the rate equations, often involving simplifying assumptions. This tried and true method makes it easy to see the logic in fitting the data and to modify and expand the model with time as new data are obtained. Moreover, the fitting is done without being tied to a particular model. However, there are two serious drawbacks to the conventional data fitting methods. First, fitting data to multiple exponential functions leads to large errors in the rates and an observed rate may not be directly related to an analytical solution involving multiple exponentials. Since the relative amplitudes and the rates of the multiple phases are allowed to float independently in the fitting process, the best fit for each curve can be quite far from the final model-dependent interpretation. This will become more apparent in the presentation of the results of the paper. Second, the simplifying assumptions needed to achieve an analytical solution to the rate equations may not be valid and with any complex pathway, secondary effects due to other kinetic steps can alter the fit to the step that is being measured. Consequently, we have chosen to follow conventional data analysis with a global fit of the data to the complete mechanism by nonlinear regression using the KINSIM and FITSIM computer simulation programs (Barshop et al., 1983; Zimmerle and Frieden, 1989).

Data fitting by computer simulation proceeds without any simplifying assumptions concerning the mechanism. The

minimal model that has been deduced by conventional data fitting is programmed into the computer, and the estimates of the rate constants from the conventional data fitting are used to predict the actual time course of the reaction as a function of concentration. The entire family of curves is then fit, allowing the less well-defined rate constants to vary to achieve the minimum sum square error to obtain the best global fit. In this process, rate constants that have been measured directly or are known with greater certainty are held fixed. The advantage of this method is that the final fit to the data is based upon the deduced mechanism and the fitting to the data includes amplitude as well as rate information to constrain the final fit to the data.

The fits obtained by such global analysis are often criticized in that the fits do not appear as good as the curves obtained by conventional fitting. However, this comparison is not valid. Consider the fits shown in Figure 2A. There are 4 curves shown which have been fit to 4 separate equations involving 4 independent parameters for a total for 16 independent parameters to fit the family of curves. In Figure 2C, the fit by global analysis is shown, and although admittedly the fit does not look as good by eye, it represents the best fit based upon nonlinear regression to the model. Moreover, it is important to note that this fit was obtained by only allowing 2 independent kinetic parameters to float in the fitting process plus 2 additional scaling factors in normalizing the data to the simulation. It is not too surprising that the fits in Figure 2A look better since 12 additional parameters have been used to achieve the observed curves. Of the 16 constants used to fit the curves in Figure 2A, only 4 are used to provide kinetic information to define the mechanism and the remainder are arbitrary fitting parameters.

Throughout the paper, we will describe the results from conventional data fitting and from global analysis to deduce the final mechanism. It is important to note that the mechanism we have deduced is decidedly incomplete. Very few reverse rates have been included and there may be additional steps in the mechanism that have not yet been resolved. The current model can be expanded as new information becomes available. For example, ATP binding may occur in two steps leading to hydrolysis. New steps can be added to the mechanism with the knowledge that any two steps in sequence need to give the same net rate constant as the one-step rate described in the current mechanism.

## RESULTS

Several experiments reported here rely upon the use of the fluorescent ATP analog mantATP. Before using mantATP in pre-steady-state kinetic studies, the analog was compared to ATP by steady-state kinetic methods (Figure 1). At a saturating concentration of microtubules, steady-state ATP hydrolysis occurs at a rate of  $84\text{ s}^{-1}$  with a  $K_{m,\text{ATP}} = 91\text{ }\mu\text{M}$ . The  $k_{\text{cat}}$  for mantATP hydrolysis at a saturating concentration of microtubules is  $89\text{ s}^{-1}$ , and  $K_{m,\text{mantATP}} = 256\text{ }\mu\text{M}$ . Similar results were obtained for the hydrolysis of ATP and mantATP by K401 (Gilbert et al., 1995). For K401 the  $k_{\text{cat}}$  for ATP and mantATP are essentially identical ( $20\text{ s}^{-1}$ ) while  $K_{m,\text{ATP}} = 61\text{ }\mu\text{M}$  and  $K_{m,\text{mantATP}} = 150\text{ }\mu\text{M}$ . The data show that the  $k_{\text{cat}}$  for mantATP is similar to that of the natural substrate, indicating that mantATP can be used as an ATP analog for K341 and K401. However, the  $K_m$

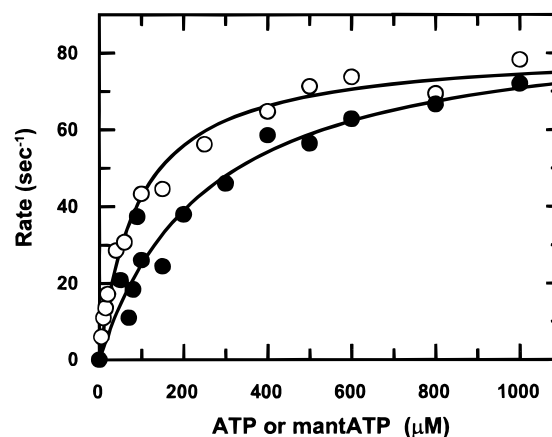


FIGURE 1: Steady-state ATP and mantATP hydrolysis activity of K341. The M•K341 complex ( $0.10\text{ }\mu\text{M}$  K341 plus  $16\text{ }\mu\text{M}$  tubulin) was formed and then incubated with ATP (○) or mantATP (●) at  $25\text{ }^{\circ}\text{C}$ . The rate of hydrolysis is shown as a function of substrate concentration. The data were fit to a hyperbola. For ATP,  $k_{\text{cat}} = 81 \pm 2\text{ s}^{-1}$  and  $K_{m,\text{ATP}} = 91 \pm 10\text{ }\mu\text{M}$ . For mantATP,  $k_{\text{cat}} = 89 \pm 8\text{ s}^{-1}$  and  $K_{m,\text{mantATP}} = 256 \pm 57\text{ }\mu\text{M}$ .

data suggest that mantATP binds the active site 2–3-fold more weakly or more slowly than ATP.

These data also show, interestingly, that the monomeric kinesin hydrolyzes ATP at a rate 4-fold faster than the dimeric kinesin. Thus, one of the goals of the work reported here is to provide an explanation for the observed activation of ATP turnover by monomeric kinesin.

**ATP Binding to Kinesin.** First, we studied the pre-steady-state kinetics of the M•K341 ATPase cycle by measuring the rate of mantATP binding. The M•K341 complex was formed with  $5\text{ }\mu\text{M}$  K341 and microtubules ( $12\text{ }\mu\text{M}$  tubulin) in excess and at a concentration shown previously to activate maximally the steady-state ATPase activity of K341 (Moyer et al., 1996). The complex was then rapidly mixed with mantATP in the stopped-flow instrument. A series of fluorescence transients are shown in Figures 2A and 2C. The binding of mantATP to the M•K341 complex gave a biphasic fluorescence change; a fast increase in fluorescence was followed by a slower decrease. Since the fluorescence of mantATP is enhanced upon K341 binding, the observed decrease in fluorescence may be correlated with a step or steps in the reaction leading to the M•K341•ADP•P<sub>i</sub> state or subsequent steps in the reaction. As described below, a global fit of the data to a complete mechanism provides an explanation for the slow phase as a function of the slower approach of the system to the steady-state distribution of kinesin–nucleotide states, without the need to invoke additional states. In Figure 2A the smooth lines show the fit of the data to an equation with one exponential term and a linear term. The rate of mantATP binding, as defined by the exponential term, is plotted as a function of the mantATP concentration in Figure 2B. The data were fit to a hyperbola to obtain the maximum rate ( $565\text{ s}^{-1}$ ) and the dissociation rate for ATP ( $112\text{ s}^{-1}$ ). The initial linear portion of the fit provides a minimum estimate for the second-order rate constant for mantATP binding of  $20\text{ }\mu\text{M}^{-1}\text{ s}^{-1}$ . These values were used as initial estimates in the KINSIM analysis (Barshop et al., 1983; Zimmerle and Frieden, 1989), which was then refined to obtain the best global fit to the data including other experimental results described below.

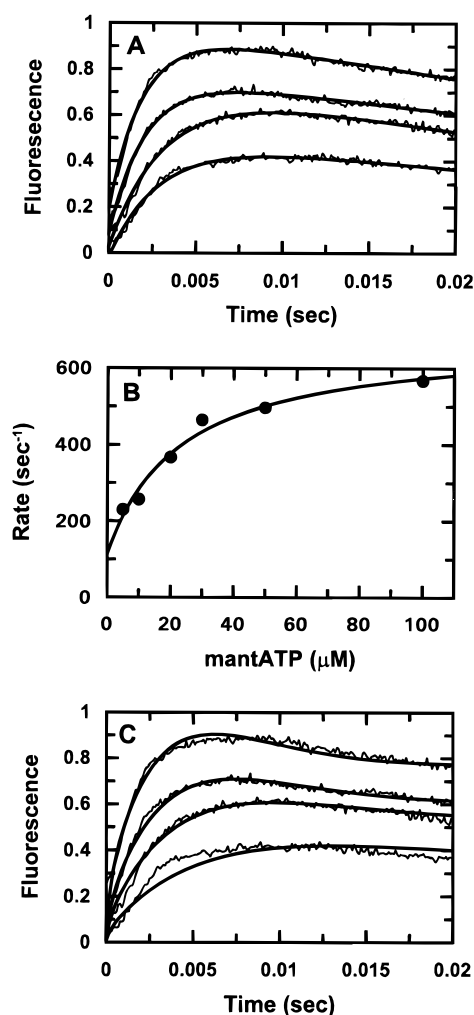


FIGURE 2: Pre-steady-state kinetics of ATP binding to the M•K341 complex. The M•K341 complex (12  $\mu$ M tubulin plus 5  $\mu$ M K341) was formed and then rapidly mixed with increasing concentrations of mantATP. All concentrations reported represent final concentrations after mixing in stopped-flow instrument. (A) Representative transients are shown for various mantATP concentrations: 10, 20, 30, and 50  $\mu$ M (from the bottom to the top trace). Fluorescence signals were normalized to show the relative change in fluorescence per K341 site. Smooth lines show the fit of the data to the burst equation ( $y = A \exp(k_b t) + k_{ss} t$ ). (B) The rate of the fast phase ( $k_b$ ) of each transient is plotted as a function of mantATP concentration. The data were fit to the equation  $k_{obs} = (k_{max}[ATP]/(K_{d,ATP} + [ATP])) + k_{off,ATP}$ . The maximum rate was  $565 \pm 50 \text{ s}^{-1}$ ,  $k_{off,ATP} = 113 \pm 60 \text{ s}^{-1}$ , and  $K_{d,ATP} = 23 \pm 10 \mu\text{M}$ . The initial linear portion of the curve predicts the apparent (minimum) second-order rate constant for mantATP binding to be  $20 \mu\text{M}^{-1} \text{ s}^{-1}$ , which is equal to  $k_{max}/K_{d,ATP}$  according to the fitted equation. Panel B includes additional data not shown in panel A. (C) Representative transients for various concentrations of mantATP as shown in (A). Smooth lines show the best global fit of the data to the mechanism in Scheme 1 with rate constants shown in Table 1.

In Figure 2C the smooth lines represent the best global fit of the data to the mechanism shown in Scheme 1 with rate constants defined in Table 1. The second-order rate constant for mantATP binding ( $k_{+1}$ ) was not changed during computer simulation from the initial estimate of  $20 \mu\text{M}^{-1} \text{ s}^{-1}$  obtained by conventional fitting of the data. The dissociation rate for mantATP ( $k_{-1}$ ) was adjusted from the initial estimate of 112 to  $200 \text{ s}^{-1}$  during computer simulation. On the basis of the rate constants determined by computer simulation, the

Scheme 1: K341 ATPase Mechanism

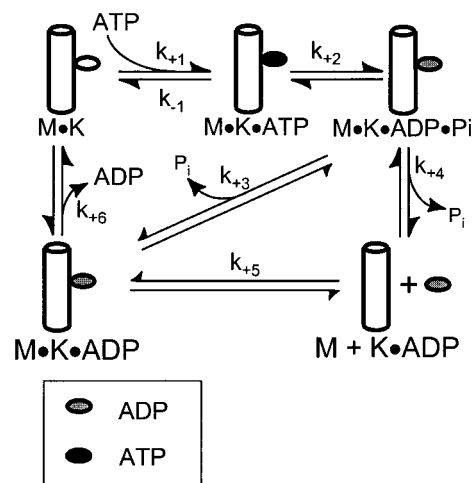


Table 1: Microtubule•K341 Kinetic Constants<sup>a</sup>

step	rate constant	source
$k_{+1}$	$20 \pm 5 \mu\text{M}^{-1} \text{ s}^{-1}$	experimentally determined (Figure 2B)
$k_{-1}$	$200 \pm 67 \text{ s}^{-1}$	experimentally determined followed by refinement by computer simulation
$k_{+2}$	$> 300 \text{ s}^{-1}$	experimentally determined followed by refinement by computer simulation (Moyer et al., 1996)
$k_{+3}$	$81 \pm 2 \text{ s}^{-1}$	based on steady-state turnover
$k_{+4}$	$9.5 \pm 0.9 \text{ s}^{-1}$ ( $11.3 \pm 0.3 \text{ s}^{-1}$ ) <sup>b</sup>	computer simulation
$k_{+5}$	$10.8 \pm 1.4 \mu\text{M}^{-1} \text{ s}^{-1}$ ( $3.8 \pm 3.5 \mu\text{M}^{-1} \text{ s}^{-1}$ ) <sup>b</sup>	experimentally determined (Figure 7B)
$k_{+6}$	$303 \pm 22 \text{ s}^{-1}$	experimentally determined (Figure 7B)

<sup>a</sup> The kinetic constants represent the best global fit of all steady-state and pre-steady-state kinetic data in ATPase buffer at 25 °C. The rate constants correspond to those in Scheme 1. <sup>b</sup> The kinetic constants represent the best global fit of all kinetic data in ATPase buffer plus 100 mM KCl at 25 °C.

calculated  $K_{d,mantATP} (k_{-1}/k_{+1})$  is approximately 10  $\mu\text{M}$ . The apparent  $K_{d,mantATP}$  predicted by conventional fitting of the data in Figure 2B is  $23 \pm 10 \mu\text{M}$ . The slower decrease in fluorescence can be understood in terms of the dissociation of mantATP at  $200 \text{ s}^{-1}$ , and the decrease in fluorescence associated with mantADP release as K341 continues through its ATP hydrolysis cycle.

The binding of mantATP to K401 was studied to compare the kinetics of mantATP binding to dimeric kinesin with the kinetics of mantATP binding to the monomer. The M•K401 complex was formed with 5  $\mu\text{M}$  K401 and microtubules (12  $\mu\text{M}$  tubulin) at a concentration at which steady-state ATP hydrolysis is activated maximally. The complex was then rapidly mixed with mantATP in the stopped-flow instrument. A series of fluorescence transients are shown in Figures 3A and 3C. The binding of mantATP to the M•K401 complex gave a fast increase in fluorescence. At higher concentrations of mantATP (30 and 40  $\mu\text{M}$ ) the increase in fluorescence is followed by a slight decrease in fluorescence, similar to the decrease in fluorescence observed with monomeric kinesin (Figures 2A and 2C). The smooth lines in Figure 3A show the fit of the data to a burst equation. Figure 3B shows the rate of the exponential term as a function of the mantATP concentration, fit to a straight line. The slope of the line defines the estimate of the second-order rate constant for

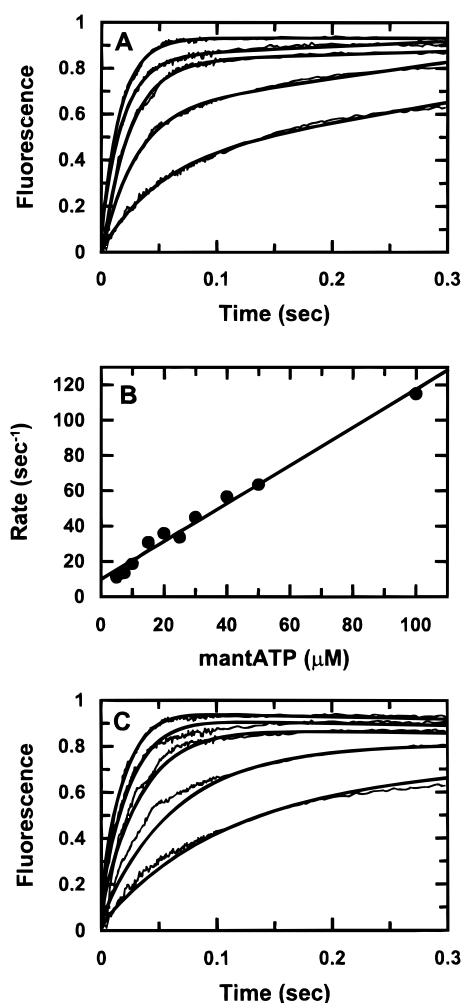


FIGURE 3: Pre-steady-state kinetics of ATP binding to the M•K401 complex. The M•K401 complex (12  $\mu\text{M}$  tubulin plus 5  $\mu\text{M}$  K401) was formed and then rapidly mixed with increasing concentrations of mantATP. (A) Transients are shown for various concentrations of mantATP: 5, 10, 20, 30, and 40  $\mu\text{M}$  (from the bottom to the top trace). Fluorescence signals were normalized to show the relative change in fluorescence per K401 site. Smooth lines show the fit of the data to the burst equation. (B) The rate of the exponential is plotted as a function of mantATP concentration. These data were fit to a straight line. The slope of the line predicts an apparent second-order rate constant for mantATP binding of  $1.1 \pm 0.04 \mu\text{M}^{-1} \text{s}^{-1}$  and a dissociation rate of  $9.8 \pm 1.9 \text{s}^{-1}$  is obtained from the intercept. Panel B includes additional data not shown in panel A. (C) Representative transients for various concentrations of mantATP as shown in (A). Smooth lines show the best global fit of the data to the mechanism in Scheme 2 with rate constants shown in Table 2.

mantATP binding to the M•K401 complex at  $1.1 \mu\text{M}^{-1} \text{s}^{-1}$ . The intercept predicts a dissociation rate for mantATP of  $10 \text{s}^{-1}$ .

Figure 3C shows the global fit of the data to the mechanism shown in Scheme 2 with rate constants defined in Table 2. Global analysis of the data suggests that the slight decrease in fluorescence that is observed can be understood in terms of the release of the fluorescent nucleotide as K401 continues through the ATP hydrolysis cycle. The predicted second-order rate constant for mantATP binding ( $k_{+8}$  as defined in Scheme 2) was adjusted from 1.1 to  $2.5 \mu\text{M}^{-1} \text{s}^{-1}$  during global analysis of the data. The predicted off-rate for mantATP ( $k_{-8}$  as defined in Scheme 2) was adjusted from 10 to  $200 \text{s}^{-1}$  by computer simulation.

Scheme 2: K401 ATPase Mechanism

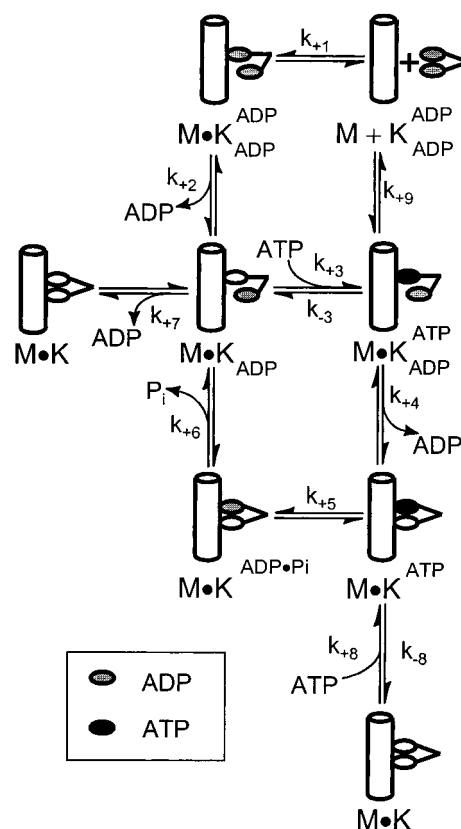


Table 2: Microtubule•K401 Kinetic Constants<sup>a</sup>

step	rate constant	source
$k_{+1}$	$19.5 \pm 0.7 \mu\text{M}^{-1} \text{s}^{-1}$	experimentally determined (Gilbert et al., 1995)
$k_{+2}$	$306 \pm 25 \text{s}^{-1}$	experimentally determined (Gilbert et al., 1995)
$k_{+3}$	$2.0 \pm 0.8 \mu\text{M}^{-1} \text{s}^{-1}$	experimentally determined followed by refinement by computer simulation
$k_{-3}$	$71 \pm 9 \text{s}^{-1}$	experimentally determined followed by refinement by computer simulation
$k_{+4}$	$300 \pm 100 \text{s}^{-1}$	computer simulation
$k_{+5}$	$100 \pm 30 \text{s}^{-1}$	experimentally determined followed by refinement by computer simulation (Gilbert & Johnson, 1994)
$k_{+6}$	$50 \pm 8 \text{s}^{-1}$	based on steady-state turnover of dimeric kinesin
$k_{+7}$	$0.4 \pm 0.1 \text{s}^{-1}$	experimentally determined followed by refinement by computer simulation (Gilbert et al., 1997)
$k_{+8}$	$2.5 \pm 1.1 \mu\text{M}^{-1} \text{s}^{-1}$	experimentally determined followed by refinement by computer simulation (Gilbert & Johnson, 1994)
$k_{-8}$	$200 \pm 100 \text{s}^{-1}$	experimentally determined followed by refinement by computer simulation (Gilbert & Johnson, 1994)
$k_{+9}$	$25 \pm 10 \text{s}^{-1}$	computer simulation

<sup>a</sup> The kinetic constants represent the best global fit of all steady-state and pre-steady-state kinetic data in ATPase buffer at 25 °C. The rate constants correspond to those in Scheme 2.

The calculated  $K_d$  ( $k_{-8}/k_{+8}$ ) for mantATP binding to the M•K401 complex is approximately 80  $\mu\text{M}$  on the basis of the rate constants defined by global analysis of the data. The  $K_d$  for ATP binding to the M•K401 complex was previously estimated to be  $\sim 100 \mu\text{M}$  in rapid quench experiments (Gilbert & Johnson, 1994). It is important to note that the kinetics of mantATP binding to monomeric K341 and

dimeric K401 differ greatly, with an apparent rate of binding 20-fold faster for K341. The significance of this difference will be discussed below.

The synthesis of mant nucleotides yields a mixture in which mant fluorophore is attached to either the 2'-hydroxyl (35%) or the 3'-hydroxyl (65%) (Cremo et al., 1990). An analog with mant fluorophore on both the 2'-hydroxyl and 3'-hydroxyl is also a byproduct of the synthesis; however, DEAE Sepharose purification separates this species from monosubstituted nucleotides (Moore & Lohman, 1994a). We also synthesized 2'-mant-3'-deoxyATP and 3'-mant-2'-deoxyATP. Binding of either mant-dATP substrate to K401 was compared to that of the mixture of the 2'- and 3'-isomers. The results show that the kinetics of mantATP binding are the same regardless of the location of mant fluorophore on the analog (data not shown).

**Phosphate Release Kinetics.** Pre-steady-state kinetics of phosphate release were measured directly using a fluorescence assay developed by Brune and co-workers by attaching a fluorescent probe (MDCC) to cysteine of the A197C mutant of *E. coli* phosphate binding protein (Brune et al., 1994). The probe (MDCC-PBP) binds phosphate tightly ( $K_d \approx 0.1 \mu\text{M}$ ) and rapidly ( $1.36 \times 10^8 \text{ M}^{-1} \text{ s}^{-1}$ ) and exhibits a 5-fold increase in fluorescence upon phosphate binding. Because this assay is so sensitive, one must eliminate trace phosphate contamination with a "phosphate mop" consisting of purine nucleoside phosphorylase and 7-methylguanosine. The equilibrium constant for this reaction is  $> 100$  (Brune et al., 1994); therefore, free phosphate in the solutions can be reduced to less than  $0.1 \mu\text{M}$ . However, the rate of phosphate reaction with the "mop" can be adjusted to be slower than the rate of phosphate binding to the phosphate binding protein, so that the kinetics of phosphate release from kinesin can be monitored. In order to convert the observed fluorescence change (volts) to phosphate concentration ( $\mu\text{M}$ ), preliminary experiments were performed in which MDCC-PBP ( $2 \mu\text{M}$ ) was rapidly mixed with known concentrations of  $\text{KH}_2\text{PO}_4$  (data not shown).

Figure 4 shows the time dependence of the fluorescence change as a measure of phosphate release from kinesin after mixing the M•K341 complex ( $0.075 \mu\text{M}$  tubulin plus  $0.05 \mu\text{M}$  K341) with ATP ( $500 \mu\text{M}$ ) in the presence and absence of  $100 \text{ mM}$  KCl. Low concentrations of microtubules and salt were used in this experiment in an attempt to slow subsequent turnovers of K341 to a steady-state rate less than the first turnover so that the burst rate and amplitude could be well defined. Solid lines show the global fit of the data to the mechanism shown in Scheme 1 with rate constants defined in Table 1. In addition, the data were analyzed by conventional fitting to a burst equation. In ATPase buffer the pre-steady-state burst rate was  $6.7 \text{ s}^{-1}$  and the burst amplitude was  $0.88 \mu\text{M}$ , approximately 18-fold larger than the K341 concentration present in the reaction. In ATPase buffer with an additional  $100 \text{ mM}$  KCl, the pre-steady-state burst rate was  $10 \text{ s}^{-1}$  and the burst amplitude was  $0.42 \mu\text{M}$ , approximately eight times the concentration of K341 present in the reaction. These data show that monomeric kinesin is capable of hydrolyzing several ATP molecules before reaching the steady-state distribution of kinesin on and off the microtubule. Thus, monomeric kinesin remains bound to the microtubule for multiple rounds of ATP hydrolysis in

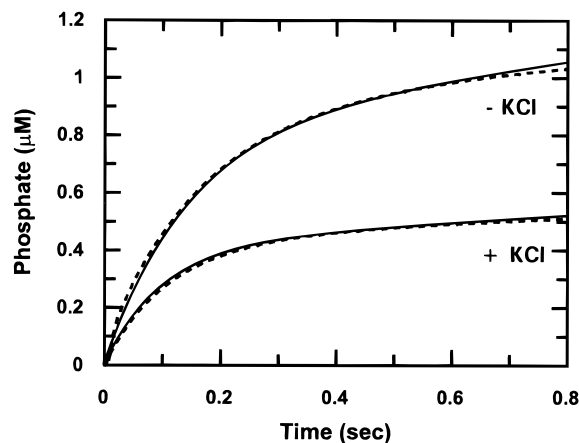


FIGURE 4: Pre-steady-state kinetics of phosphate release from the M•K341 complex. Phosphate release kinetics were measured using a fluorescence assay (Brune et al., 1994). The M•K341 complex ( $0.05 \mu\text{M}$  K341 plus  $0.075 \mu\text{M}$  tubulin) was rapidly mixed with  $500 \mu\text{M}$  ATP in the presence or absence of  $100 \text{ mM}$  KCl. Each stopped-flow syringe contained  $2 \mu\text{M}$  fluorescently labeled phosphate binding protein (MDCC-PBP) and a "phosphate mop" consisting of  $0.03 \text{ u/mL}$  purine nucleoside phosphorylase and  $0.1 \text{ mM}$  7-methylguanosine. The figure shows the time course of phosphate release. The data are shown by a dashed line while the smooth line shows the fit of the data to the mechanism in Scheme 1 with rate constants in Table 1. Conventional fitting to a pre-steady-state burst equation yields an amplitude of  $0.830 \pm 0.004 \mu\text{M}$  (17.6 per site) and a burst rate =  $6.73 \pm 0.06 \text{ s}^{-1}$  in ATPase buffer. In ATPase buffer plus  $100 \text{ mM}$  KCl the pre-steady-state burst amplitude was  $0.430 \pm 0.002 \mu\text{M}$  (8 per site) and the burst rate was  $8.90 \pm 0.01 \text{ s}^{-1}$ .

the presence and absence of added KCl leading to a superstoichiometric phosphate burst.

**ATP-Promoted Dissociation of M•K341 Complex.** We measured K341 dissociation from the microtubule directly by stopped-flow light-scattering measurements. The M•K341 complex ( $1.5 \mu\text{M}$  K341 plus  $1.35 \mu\text{M}$  tubulin) was rapidly mixed with ATP in the presence of  $100 \text{ mM}$  KCl. Figure 5A shows the time course of K341 dissociation measured by turbidity. The data were fit to a burst equation ( $y = A \exp(k_{bt}) + k_{ss}t$ ). The rate of the linear phase was independent of ATP concentration and too slow ( $0.1 \text{ s}^{-1}$ ) to be a part of the ATPase cycle. The linear phase was attributed to disassociation of other aggregates in solution and/or microtubule disassembly and was therefore ignored. Dissociation of K341 from the microtubule was also determined by measuring the rate of fluorescence decrease as K341 was released from microtubules labeled 1:1 with dansyl chloride. The decrease in fluorescence observed as K341 dissociates from the labeled microtubules is shown in Figure 5B. The smooth line in Figure 5B shows the fit of the data to the burst equation. The rate of the burst was measured as a function of the ATP concentration by light scattering and by fluorescence (Figure 5C). The maximum rates of dissociation measured by light scattering and by fluorescence were  $22.5 \pm 1.4$  and  $21.1 \pm 0.8 \text{ s}^{-1}$ , respectively.

A change in turbidity or fluorescence was not observed when M•K341 was mixed with ATP in the absence of  $100 \text{ mM}$  KCl; the amplitude of the dissociation reaction was too small to observe. A number of experiments were performed in the presence a higher salt concentration to weaken the binding of kinesin to the microtubules so that dissociation

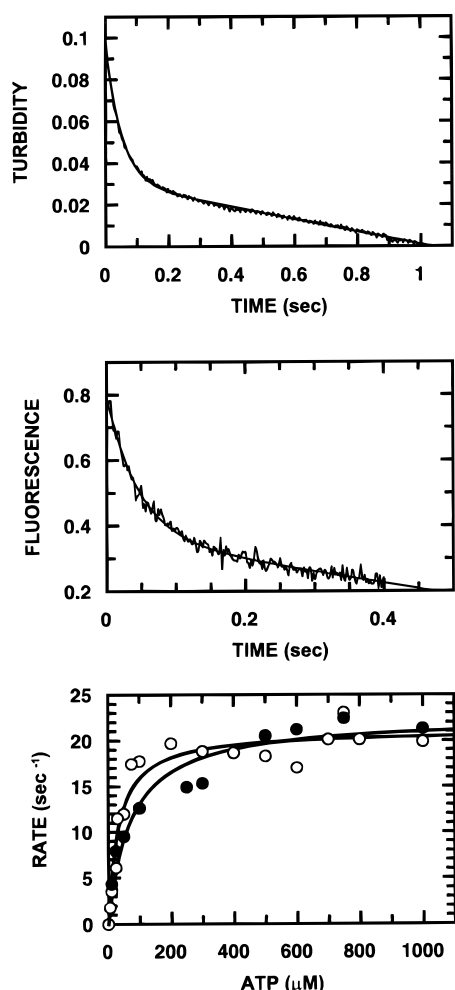


FIGURE 5: Dissociation of M•K341 Complex. (A) Representative stopped-flow record obtained after mixing M•K341 (1.5  $\mu\text{M}$  K341 plus 1.35  $\mu\text{M}$  tubulin) with 1 mM ATP plus 100 mM KCl. The data were fit to the burst equation ( $Y = A \exp(k_b t) + k_{ss} t$ ) with  $k_b = 21.3 \pm 0.2 \text{ s}^{-1}$ . The slow phase of the reaction was attributable to other reactions such as microtubule disassembly or dissociation of other higher order aggregates and was, therefore, ignored. (B) Representative stopped-flow record obtained after mixing M•K341 (1.5  $\mu\text{M}$  K341 plus 1.35  $\mu\text{M}$  tubulin labeled 1:1 with dansyl chloride) with 1 mM ATP plus 100 mM KCl. The data were fit to the burst equation with  $k_b = 21.4 \pm 1.0 \text{ s}^{-1}$ . (C) The pre-steady-state burst rates obtained by light scattering (○) and fluorescence (●) plotted as a function of ATP concentration. The data were fit to hyperbola. The maximum rates of dissociation were  $22.5 \pm 1.4 \text{ s}^{-1}$  by light scattering and  $21.1 \pm 0.8 \text{ s}^{-1}$  by fluorescence. Half-maximal rates of dissociation occurred at ATP concentrations of  $72 \pm 20 \mu\text{M}$  by light scattering and  $33 \pm 7 \mu\text{M}$  by fluorescence.

of the kinesin could be observed and measured. Therefore, we determined the effect of salt on ATP turnover by steady-state and rapid-quench methods. Rapid-quench experiments indicate that the kinetics of ATP hydrolysis by the M•K341 complex during the first turnover were not affected by the addition of 100 mM KCl (data not shown). Steady-state results in the presence of 100 mM KCl show that subsequent turnovers of K341 are affected by the presence of additional salt (data not shown). In ATPase buffer  $k_{\text{cat}}$  is  $81 \pm 3 \text{ s}^{-1}$  whereas in ATPase buffer plus 100 mM KCl  $k_{\text{cat}}$  is  $69 \pm 7 \text{ s}^{-1}$ . The apparent affinity of K341 for the microtubule is significantly affected by additional salt. The  $K_{0.5, \text{MT}}$  in ATPase buffer is  $3.1 \pm 0.4 \mu\text{M}$ . In ATPase buffer plus 100 mM KCl  $K_{0.5, \text{MT}}$  is  $16 \pm 4 \mu\text{M}$ . These rapid quench and

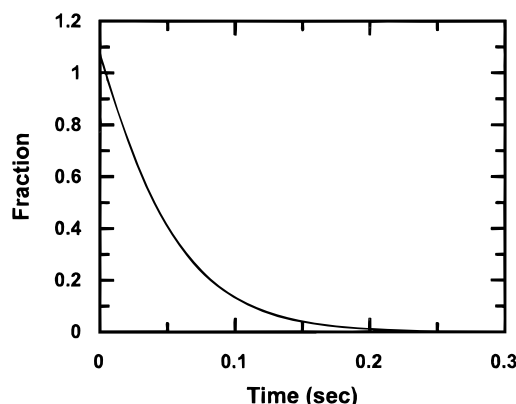


FIGURE 6: Simulated kinetics of M•K341 dissociation. The KINSIM kinetic modeling program and the mechanism shown in Scheme 1 were used to simulate dissociation of the M•K341 complex. Simulation parameters are as follows: M•K341 complex consisting of 1.35  $\mu\text{M}$  tubulin plus 1.5  $\mu\text{M}$  K341, 500  $\mu\text{M}$  ATP, and 100 mM KCl. The rate constants used in this simulation are those shown in Table 1 under high salt conditions. Simulation of the decrease in the fraction of K341 bound to the microtubule as a function of time is shown. Simulated kinetics predict a rate of  $19 \text{ s}^{-1}$  for K341 dissociation from the microtubule.

steady-state results indicate that additional KCl does not greatly affect ATP binding or hydrolysis but does significantly affect rebinding of K341 to the microtubule.

Steady-state experiments performed with dansyl chloride labeled microtubules show that the label does not affect binding of K341 to the microtubule. The maximum rate of ATP hydrolysis in the presence of dansyl chloride labeled microtubules and 100 mM KCl was  $60 \pm 3 \text{ s}^{-1}$  and the  $K_{0.5, \text{MT}}$  for labeled microtubules was  $11.0 \pm 1.2 \mu\text{M}$  (data not shown).

The results presented here demonstrate that kinesin does not dissociate from the microtubule after a single ATP turnover. Accordingly, one can understand the apparently contradictory results whereby the pre-steady-state burst rate is slower than steady-state turnover since the pre-steady-state reaction represents multiple turnovers as the system approaches the steady state. To more rigorously analyze the kinetics of this complex process, the KINSIM kinetic modeling program and the mechanism shown in Scheme 1 were used to simulate K341 dissociation from the microtubule. The simulation shown in Figure 6 was performed using the conditions of the experiment shown in Figure 5 and the rate constants given in Table 1. Figure 6 shows the predicted decrease in K341 bound to the microtubule as a function of time. Simulated kinetics predict a rate of  $19 \text{ s}^{-1}$  for K341 dissociation from the microtubule. Computer simulation, therefore, accounts for the slow rate of K341 dissociation from the microtubule as occurring during multiple turnovers of ATP. The observed rate of K341 dissociation from the microtubule and the observed steady-state rate are reconciled by considering the ability of K341 to hydrolyze several ATP molecules before dissociating from the microtubule. A similar analysis accounts for the kinetics observed with dimeric K401 as described below.

**ADP Release Kinetics in the Presence of Microtubules.** We measured the rate of ADP release from K341 using mantADP. ADP at the active site of K341 was exchanged with mantADP by incubating mantADP with K341. K341•mantADP was then rapidly mixed with microtubules in the



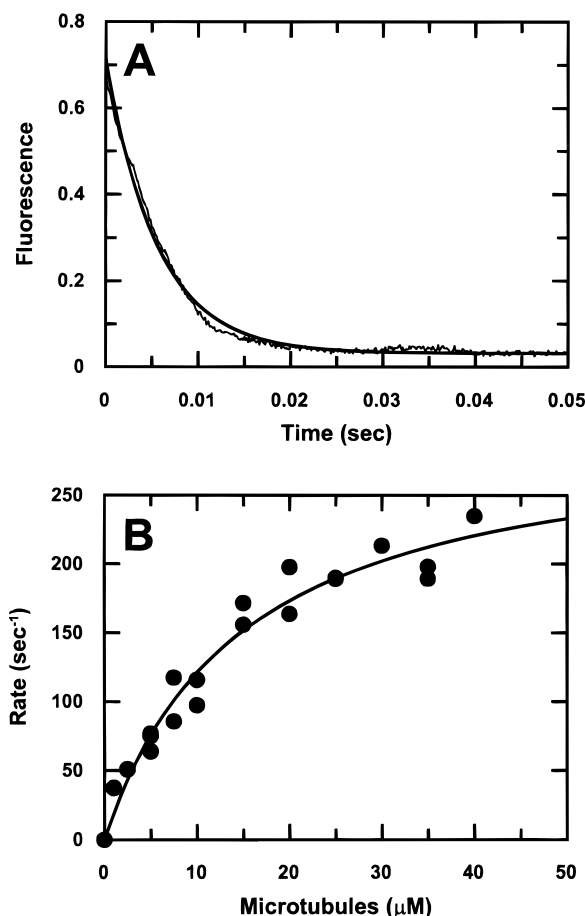


FIGURE 7: Release of mantADP from M•K341•mantADP complex. (A) A stopped-flow time course after mixing 2  $\mu\text{M}$  K341•4  $\mu\text{M}$  mantADP with microtubules (10  $\mu\text{M}$  tubulin) plus 1 mM ATP. The data were fit to a single exponential with  $k_{\text{obs}} = 164 \pm 2 \text{ s}^{-1}$ . (B) The rate of mantADP release was plotted as a function of tubulin concentration. The data were fit to a hyperbola with maximum rate of mantADP release  $303 \pm 22 \text{ s}^{-1}$  and a microtubule concentration giving a half-maximal rate equal to  $15.0 \pm 2.5 \mu\text{M}$ .

presence of 1 mM ATP. Figure 7A shows the time dependence of the fluorescence change. The data were fit to a single exponential to get the results shown in Figure 7B. The rate of mantADP release increased as a function of microtubule concentration and was fit to a hyperbola to define a maximum rate of release of mantADP of  $303 \text{ s}^{-1}$ . The slope of the initial linear portion of the curve predicts a second-order rate constant of  $11 \mu\text{M}^{-1} \text{ s}^{-1}$  as a minimum estimate for the rate of microtubule binding. The experiment was repeated by rapidly mixing K341•mantADP with microtubules in the absence of ATP. The kinetics of mantADP release are identical regardless of the presence or absence of ATP (see Gilbert et al., 1998).

ADP release kinetics were also determined by monitoring the binding of mantATP to K341 after mixing K341 (with ADP bound at the active site) with microtubules plus mantATP.

Figure 8 shows a series of fluorescent transients at various concentrations of mantATP. The smooth lines represent the global fit of the data to Scheme 1. A lag in the fluorescence increase is observed in this experiment which reflects the time required for K341 to bind to the microtubule and release ADP before mantATP can bind the active site of K341. This lag is predicted from the mechanism shown in Scheme 1

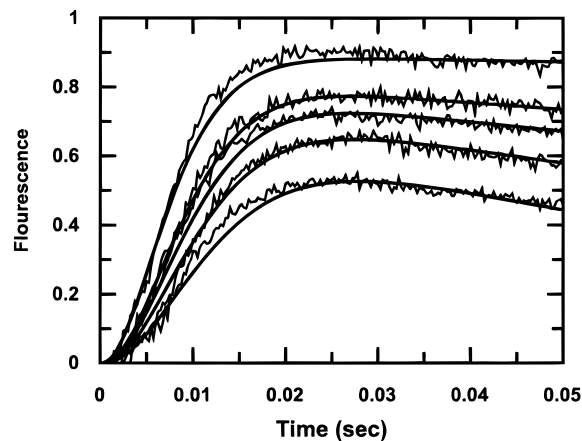


FIGURE 8: ADP release kinetics determined by binding of mantATP to K341. K341 (5  $\mu\text{M}$  with ADP bound at the active site) was rapidly mixed with microtubules (12  $\mu\text{M}$  tubulin) plus increasing concentrations of mantATP. The figure shows the transients for various mantATP concentrations: 10, 15, 20, 25, and 50  $\mu\text{M}$  (from the bottom to the top trace). Fluorescence signals were normalized to show the relative change in fluorescence increase per K341 site. Smooth lines show the best fit of the data to the mechanism shown in Scheme 1 with rate constants shown in Table 1.

and supports the interpretation that the kinetics of mantADP release at  $303 \text{ s}^{-1}$  represents the kinetics of ADP release from the M•K341 complex.

The kinetics of ADP release were also determined by binding of mantATP to dimeric kinesin in an experiment where K401 (with ADP bound at the active site) was rapidly mixed with microtubules and increasing concentrations of mantATP. In this experiment the ATP hydrolysis cycle is entered from a different experimentally accessible point than in the experiment in which mantATP binding to the M•K401 complex was studied. In this experiment, the hydrolysis cycle is entered as K401 binds to the microtubule and releases ADP (steps 1 and 2 of Scheme 2). In the experiment in which mantATP binding to the M•K401 complex is studied the hydrolysis cycle is entered by binding mantATP (step 8 of Scheme 2). A lag in the increase in fluorescence is observed which reflects the time required for K401 to bind to the microtubule and release ADP before mantATP can bind to the active site of K401 (Figure 9). The experiment allows one to estimate the rate of ADP release followed by the rate of mantATP binding. Global analysis of these results supports our interpretation that the kinetics of ADP release are fast (Gilbert et al., 1995). Furthermore, the analysis defines the kinetics of mantATP binding to one motor domain of K401 while the second motor domain of the dimer is not bound to the microtubule. The second-order rate constant for mantATP binding to the active site of the first motor domain while ADP is bound to the active site of the second motor domain ( $k_{+3}$  as defined in Scheme 2) is predicted to be approximately  $2 \mu\text{M}^{-1} \text{ s}^{-1}$  while the off-rate ( $k_{-3}$  as defined in Scheme 2) is predicted to be approximately  $71 \text{ s}^{-1}$ . The  $K_d$  calculated for mantATP binding to this intermediate is therefore approximately  $36 \mu\text{M}$ .

The experiment described in Figure 9 was repeated with 2'-mant-3'-dATP and 3'-mant-2'-dATP. Binding of both mant-dATP substrates to K401 was compared to that of the mixture of the 2'- and 3'-isomers. No difference in the kinetics was observed, indicating that the kinetics of mantATP binding

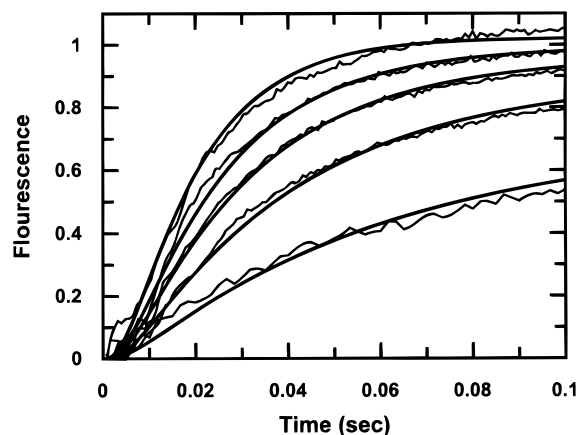


FIGURE 9: ADP release kinetics determined by binding of mantATP to K401. K401 (5  $\mu\text{M}$  with ADP bound at the active site) was rapidly mixed with microtubules (12  $\mu\text{M}$  tubulin) with increasing concentrations of mantATP. The figure shows the transients for various mantATP concentrations: 5, 10, 15, 20, and 30  $\mu\text{M}$  (from the bottom to the top trace). The fluorescence signals were normalized to show the relative change in fluorescence increase per K401 site. Smooth lines show the best global fit of the data to the mechanism shown in Scheme 2 with rate constants shown in Table 2.

are the same regardless of the location of mant fluorophore on the analog (data not shown).

## DISCUSSION

The results presented here have defined the steps of the ATPase cycle of monomeric kinesin and have extended the definition of the ATPase cycle of dimeric kinesin. The kinetics of mantATP binding to the M•K341 complex, release of phosphate and ADP from K341, and dissociation of the M•K341 complex were measured directly. Kinetic simulation of all data collected supports our model of ATP hydrolysis by monomeric K341 as shown in Scheme 1 with rate constants shown in Table 1. In addition, we have included new rate measurements on the dimeric K401 and analyzed these data globally with previously published work to provide the model shown in Scheme 2 with rate constants summarized in Table 2. These data taken together define the pathway by which kinesin couples ATP hydrolysis to force production by an alternating site mechanism.

The mechanism shown in Scheme 1 illustrates the elementary steps in the reaction pathway for K341. After ATP binds to the M•K341 complex and is hydrolyzed, the M•K341 ATPase cycle is completed in one of two ways. The K341•ADP•P<sub>i</sub> complex may dissociate from the microtubule and release phosphate, and then the K341•ADP intermediate will rebind the microtubule and release ADP to complete the cycle. Alternatively, K341 may remain bound to the microtubule and complete the ATPase cycle by release of phosphate and ADP without dissociation from the microtubule. Indeed, both pathways operate, but the latter predominates for the monomeric K341. The constants shown in Table 1 illustrate the kinetic partitioning of the K341•ADP•P<sub>i</sub> intermediate leading to partial dissociation during each cycle accounting for a burst amplitude of 18 molecules of ATP per kinesin site during the approach to steady state. Direct measurement of the rate of dissociation of K341 from the microtubule supports this interpretation.

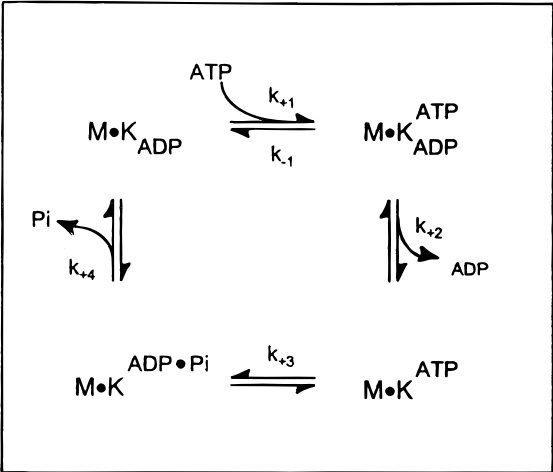
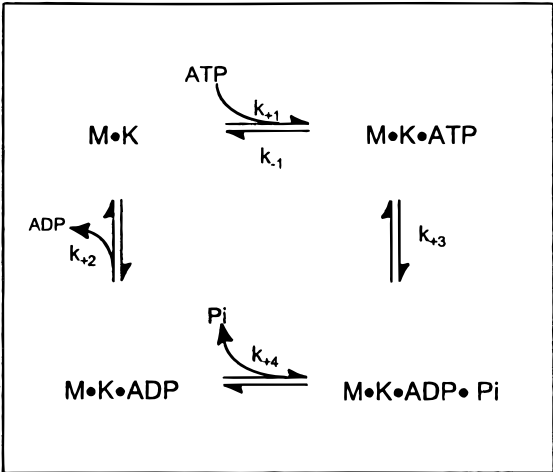
A model of coordinated ATP hydrolysis by dimeric K401 has been presented on the basis of experiments in which

biphasic release of mantADP was observed (Gilbert et al., 1998). The results presented here confirm and extend this model as summarized in Scheme 2 where we illustrate the experimentally accessible entry points of the cycle. For example, we can enter the cycle by binding dimeric kinesin (with ADP bound) from solution such that the first motor domain binds to the microtubule leading to rapid ADP release. ATP then binds to the newly vacated active site and thereby stimulates rapid ADP release from the second kinesin motor domain. ATP hydrolysis occurs on the first head followed by the rate-limiting step that results in dissociation of the first motor domain from the microtubule coupled to phosphate release. The cycle is then repeated for the second motor domain. Processivity of the dimeric K401 is a function of slower reactions leading to the release of both heads from the microtubule by the pathways illustrated in Scheme 2 and resulting in complete dissociation of the kinesin from the microtubule.

The mechanisms shown for monomeric and dimeric kinesin represent the best fit of all steady-state and pre-steady-state data presented in this report and in previously published work (Gilbert et al., 1995; Gilbert & Johnson, 1994; Gilbert et al., 1998; Moyer et al., 1996). The mechanisms are by no means complete. Rather, the schemes represent the minimal mechanism determined for the ATP hydrolysis pathways for K341 and K401, sufficient to account for the data. There are points in the mechanisms that are still unresolved. Most notably we have not yet resolved whether phosphate release occurs before or after dissociation of kinesin from the microtubule since phosphate release and dissociation of kinesin from the microtubule occur at the same rate. Furthermore, the models presented do not include any conformational changes that may take place at several points in the ATP hydrolysis cycle for both monomeric and dimeric kinesin. For example, the rate of the fluorescence change upon mantATP binding to the M•K341 complex saturated at a rate of approximately 600 s<sup>-1</sup>, which could be a conformational change in the protein after ATP binding or changes in fluorescence during ATP hydrolysis in the pathway. However, a rate of 600 s<sup>-1</sup> is too fast to be resolved in the quench-flow experiment to measure hydrolysis directly. Another shortcoming of the models presented is that very few reverse rates have been included. Therefore, calculation of the steady-state parameters based on the models shown does not necessarily correspond to the measured steady-state rates observed. Experiments are underway to define the reversible steps in the mechanism and to resolve additional steps in the ATP hydrolysis pathway for K341 and K401. The mechanisms shown represent the simplest schemes necessary to explain the data that have been collected to date. The models presented are meant to serve as foundations for further investigation of the ATP hydrolysis and force production cycle of this very complex enzyme. Additional steps and/or reverse rates may be added as new data become available.

Comparison of the kinetics seen with monomeric and dimeric kinesin molecules reveals new features of the coupling mechanism. There are three remarkable features of the ATPase reaction catalyzed by the monomeric K341 as compared to the dimeric K401: (1) the monomeric kinesin hydrolyzes ATP without dissociating from the microtubule, (2) the rate of steady-state turnover is 4-fold faster for

Table 3: Kinetics of Monomeric and Dimeric Kinesin<sup>a</sup>

	Dimeric Kinesin			Monomeric Kinesin		
						
	$k_{+1}$ ( $\mu\text{M}^{-1} \text{s}^{-1}$ )	$k_{-1}$ ( $\text{s}^{-1}$ )	$k_2$ ( $\text{s}^{-1}$ )	$k_3$ ( $\text{s}^{-1}$ )	$k_4$ ( $\text{s}^{-1}$ )	$k_{\text{cat}}^b$ ( $\text{s}^{-1}$ )
K401	2	71	300	150	50	20
K341	20	200	300	>300	80	80

<sup>a</sup> The scheme depicts the steps in the ATPase pathway for monomeric and dimeric kinesin with rate constants defined in the table. For dimeric kinesin, one turnover of ATP requires one and one-half turns of the ATPase cycle shown. <sup>b</sup> Maximum steady-state rate of ATP hydrolysis per enzyme active site.

monomeric kinesin, and (3) the rate of ATP binding to monomeric kinesin is 10-fold faster (see Table 3). Truncation of the protein to produce the monomeric K341 results in loss of cooperative interactions between the monomer units of the dimer and loss of processive motility. Therefore these data suggest several important aspects of the coordination of the ATPase cycles between the two heads. One must consider that the truncation of the protein could result in loss of structural elements necessary for ATP binding and hydrolysis, and therefore the kinetic analysis of the monomer may be largely meaningless. However, a closer inspection of the data argues against this view. Since there is direct evidence for alternating site activity in the dimer and the monomer shows rates of ATP binding and steady-state turnover faster than the dimer, these data argue strongly for a functional significance to the changes in the kinetic constants seen in the monomer, reflecting aspects of the alternating site mechanism of the dimer. Accordingly, these data suggest that cooperative interactions between the monomer units of the dimer lead to inhibition of the rate of ATP binding and the rate of steady-state turnover and facilitate the release of one monomer unit from the microtubule dependent upon reactions occurring on the other monomer unit. These postulates will be described in more detail below.

The slow rate of dissociation of the monomer from the microtubule suggests that one function of cooperative interactions between the monomer units of the dimer is to facilitate the alternating release of the kinesin heads from the microtubule during processive movement. Accordingly, it is important to distinguish processive ATP hydrolysis by kinesin from the ability of kinesin to support concerted movement. Biochemically, processivity is defined by the number of ATP molecules hydrolyzed per encounter of

kinesin with the microtubule, while processivity observed by motility assays is based on the observation that kinesin may translocate for long distances along the surface of a microtubule before being released. A single dimeric kinesin molecule has been observed to move several micrometers along the surface of a microtubule before dissociating (Howard et al., 1989; Block et al., 1990). However, in motility assays with monomeric kinesin constructs, motility is only observed when a large number of kinesin molecules are present and the movement is erratic and extremely slow, more akin to a biased random walk (Berliner et al., 1995; Vale et al., 1996; Stewart et al., 1993). To date there are no data to support directed movement of single monomeric kinesin molecules. The analysis presented here suggests that monomeric kinesin will stay bound to the surface of the microtubule while undergoing multiple rounds of ATP hydrolysis without processive movement. Thus, the “processivity” of the monomeric kinesin is not a function of it hopping along the microtubule surface, rather it simply does not dissociate. The minimal movement seen at high surface densities of monomeric kinesin may be due to conformational changes occurring during the ATPase cycle and the slow release of each head from the microtubule. Moreover, it may reflect some cooperativity among the multiple kinesin molecules interacting with a single microtubule.

The results presented here on the dimer reveal an additional feature of this alternating site mechanism, namely, reactions occurring on one head facilitate the release of the neighboring head from the microtubule. Although the data cannot unequivocally establish the state of the neighboring head while one head is being pulled from the microtubule, a reasonable postulate can be put forth. Assuming that the rate-limiting step in ATP turnover is the release of the kinesin from the microtubule after ATP hydrolysis to form the K•

ADP·P<sub>i</sub> state, while this is occurring, the other head is binding to the microtubule and releasing its tightly bound ADP. Thus, it is reasonable to suppose that the tight binding of one head to the microtubule is coupled to the release from the microtubule of the head in the K·ADP·P<sub>i</sub> state. This postulate solves an important dilemma in defining the force-producing state in the kinesin alternating site ATPase mechanism. Our previous analysis showed that the release of K·ADP·P<sub>i</sub> from the microtubule could be the rate-limiting step in the mechanism (Gilbert et al., 1995). Although it is reasonable to suggest that the slowest step in the pathway is involved in force production, it is not reasonable to propose that force is produced in a step leading to release of the kinesin from the microtubule. Rather, the production of force must occur in a step leading to tight binding to the microtubule. However, the release of ADP from kinesin upon binding to the microtubule is too fast to be involved in force production directly. The current model solves these problems by postulating that force is produced by the interaction of the head binding to the microtubule (and releasing its ADP), but the rate of force production is governed by the release of the neighboring head from the microtubule. Accordingly, the alternating site mechanism provides a reasonable basis for force production by coupling ATP binding and hydrolysis on one head to the release of ADP and force production by the neighboring head. Keeping the reactions on the two heads out of phase from each other ensures an efficient, processive movement of kinesin along the microtubule surface.

The alternating site mechanism is the central feature of the ATP hydrolysis pathway for dimeric kinesin, whereby ATP binding to one site is coupled to ADP release from the neighboring site (Table 3). The observed 10-fold slower rate of ATP binding to the dimer as compared to that of the monomer may be a function of the negative cooperativity between the two monomer units. That is, one may postulate that if ATP binding to one site is coupled to an unfavorable structural transition in the neighboring site, then one might expect that the interaction between the neighbors would lead to weaker and perhaps slower binding of ATP. Thus, the observed 10-fold slower binding of ATP to K401 compared to K341 may be a function of the negative interactions between the subunits of the dimer.

Monomeric forms of kinesin have been shown to have higher ATPase rates (Moyer et al., 1996; Lockhart et al., 1995; Huang & Hackney, 1994; Hackney, 1994b; Ma and Taylor, 1997a; Rosenfeld et al., 1996) than dimeric forms of kinesin. However, most of the difference in steady-state turnover rates comparing monomer and dimer can be accounted for by the alternating site mechanism shown to operate with the dimer. As shown in Scheme 2, the 20 s<sup>-1</sup> steady-state turnover rate per monomer unit within the dimer requires a minimum rate of 50 s<sup>-1</sup> during each cycle since only one monomer is active at a time and other steps are partially rate limiting. Thus, one is left to explain a difference between K401 and K341 of only 50 and 80 s<sup>-1</sup>, and such a small difference in rates may not warrant more complex mechanistic conclusions. That is, the majority of the observed enhancement of steady-state ATPase rates observed with the monomer is due to the alternating site mechanism and the cooperative interactions which suppress ATP turnover by one subunit at a time in the dimer.

Phosphate release experiments have provided direct evidence that monomeric kinesin hydrolyzes several ATP molecules before steady-state distribution of kinesin on and off the microtubule is attained. The amplitudes of the phosphate release transients are greater than the concentration of monomeric kinesin present in the reaction and reflect the processivity of the ATPase cycles. It has been reported previously that under low salt conditions dimeric K401 hydrolyzes 10 molecules of ATP per kinesin head before complete release from the microtubule (Gilbert et al., 1995). The previous report indicated that K401 was not processive under high salt conditions. Analysis of the data presented previously and extended to longer reaction times by global fitting to the mechanism shown in Scheme 2 has led to an adjustment in the estimated number of ATP molecules hydrolyzed by K401 before its release from the microtubule. This analysis indicates that under low salt conditions K401 hydrolyzes ~5 ATP molecules per kinesin motor domain. At higher salt concentrations ATP hydrolysis is reduced to 3 ATP molecules per active site. This analysis also accounts for the slow rate of the phosphate burst as due to multiple turnovers prior to reaching steady state.

Phosphate release experiments with K341 indicate that monomeric kinesin hydrolyzes more ATP molecules while bound to the microtubule than does K401. Under low salt conditions K341 hydrolyzes 18 ATP molecules per kinesin motor domain before dissociating from the microtubule. At a higher salt concentration 8 molecules of ATP are hydrolyzed before steady-state distribution of K341 on and off the microtubule is attained. Monomeric kinesin hydrolyzes more ATP per encounter with the microtubule than does dimeric kinesin. This phenomena reflects the interactions between the subunits of the dimer which facilitate the alternating release of kinesin heads during processive movements by dimeric kinesin.

Hackney has proposed that a dimeric kinesin construct is processive on the basis of its tight binding to microtubules and high ATPase rates in the presence of microtubules (Hackney, 1995a; Hackney, 1995b). He suggests that DKH392, a dimeric kinesin construct from *Drosophila*, hydrolyzes more than 100 molecules of ATP per encounter with the microtubule. Hackney's estimate of processivity is based upon a comparison of the apparent second-order rate constant for microtubule binding obtained from steady-state measurements ( $k_{cat}/K_{0.5,MT}$ ) with the observed second-order rate constant for kinesin association with the microtubule. Similar analysis of other truncated kinesin constructs ranging in length from 346 amino acids to 405 amino acids suggests that monomeric kinesin constructs hydrolyze approximately 4 ATP molecules per encounter with the microtubule (Jiang et al., 1997).

Rapid quench experiments, designed to measure the production of ADP or phosphate upon ATP hydrolysis, have been performed with monomeric kinesin constructs by Jiang & Hackney (1997) and Ma & Taylor (1997a). Both groups have reported a superstoichiometric burst of phosphate of approximately 1.2–2 phosphate per enzyme active site similar to results reported with K341 (Moyer et al., 1996) and suggesting a processivity, in terms of ATP molecules hydrolyzed before dissociation of kinesin from the microtubule, of approximately 2. However, the burst amplitude observed in the phosphate release experiments reported here

is approximately 18 per K341 active site. The difference in the two measurements is a function of the microtubule concentration used during the experiment. In the rapid quench experiments, high microtubule concentrations are required to see the burst reaction, and as the system approaches the steady state, there is still a high degree of association of the kinesin with the microtubule. Therefore, the amplitude of the burst is only slightly greater than one. In contrast, the fluorescence phosphate release assay provides such extraordinary sensitivity that the burst can be measured at much lower microtubule concentrations and so the amplitude of the transient is much larger because the system approaches a steady-state distribution with far less kinesin bound to the microtubule. This experiment provides a more accurate assessment of the processivity.

Transient kinetic analysis of DKH357 suggests a model for the ATP hydrolysis pathway for monomeric kinesin whereby the motor domain completes 2–4 sequential ATP hydrolysis cycles, in which ATP hydrolysis is the major rate-limiting step, before dissociation from the microtubule (Jiang & Hackney, 1997). Ma and Taylor have proposed a model for the ATP hydrolysis cycle for monomeric kinesin in which rate-limiting phosphate release occurs prior to dissociation of HK332-ADP from the microtubule (Ma & Taylor, 1997a), based upon their observation of a burst amplitude of 2.

There is general agreement that the kinesin ATPase follows an alternating site mechanism that contains at least some elements of the model first proposed by Hackney (1994a). Recent work by Ma and Taylor (1997b) and the data presented here greatly expand the support for and significantly extend the details of the alternating site mechanism. The data presented by the three laboratories lead to similar models that differ largely in the extent to which ADP release is rate limiting. Hackney has suggested that ADP release may be entirely rate limiting and Ma and Taylor suggest that it is partially rate limiting, while our data suggest that ADP release is not at all rate limiting. However, even though the rates of specific steps differ between laboratories, all of the models suggest an alternating site mechanism in which the ATPase cycles of the two motor domains are out of phase (Ma & Taylor, 1997b; Hackney, 1994a; Jiang et al., 1997; Gilbert et al., 1998). This is the essential distinguishing feature of the kinesin ATPase.

The present study has defined the ATPase mechanism for monomeric kinesin. The results show that K341 is capable of hydrolyzing several ATP molecules before steady-state distribution of kinesin on and off the microtubule is reached. Monomeric kinesin binds the microtubule and undergoes repeated rounds of ATP hydrolysis but does not dissociate and rebind as part of the cycle. We propose that the second motor domain is necessary in order to pull the first kinesin motor domain off the microtubule as part of the normal force-producing cycle. The accompanying report shows that ATP binding to one kinesin head induces the binding of the adjacent head to the microtubule with the subsequent release of ADP. In this report the results imply that the binding of one kinesin head to the microtubule facilitates the release of the adjacent head (the one the just bound and hydrolyzed ATP). Thus, these two interactions between the two kinesin heads help to keep the ATPase cycles out of phase with each other and coupled to binding and release from the microtubules to allow an alternating site mechanism for movement

along the surface of the microtubule. Cooperative interaction between the kinesin motor domains is required to produce the distinctive processive motility behavior of kinesin.

## ACKNOWLEDGMENT

The authors sincerely thank Drs. Martin Webb and Martin Brune (National Institute for Medical Research, Mill Hill) for providing the modified phosphate binding protein.

## REFERENCES

- Barshop, B. A., Wrenn, R. F., & Frieden, C. (1983) *Anal. Biochem.* 130, 134–145.
- Berliner, E., Young, E. C., Anderson, K., Mahtani, H. K., & Gelles, J. (1995) *Nature* 373, 718–721.
- Block, S. M., Goldstein, L. S. B., & Schnapp, B. J. (1990) *Nature* 348, 348–352.
- Bloom, G. S., Wagner, M. C., Pfister, K. K., & Brady, S. T. (1988) *Biochemistry* 27, 3409–3416.
- Borisy, G. G., Olmsted, J. B., Marcum, J. M., & Allen, C. (1974) *Fed. Proc. Fed. Am. Soc. Exp. Biol.* 33, 167–174.
- Brune, M., Hunter, J. L., Corrie, J. E. T., & Webb, M. R. (1994) *Biochemistry* 33, 8262–8271.
- Correia, J. J., Gilbert, S. P., Moyer, M. L., & Johnson, K. A. (1995) *Biochemistry* 34, 4898–4907.
- Cremo, C. R., Neuron, J. M., & Yount, R. G. (1990) *Biochemistry* 29, 3309–3319.
- Gilbert, S. P., Webb, M. R., Brune, M., & Johnson, K. A. (1995) *Nature* 373, 671–676.
- Gilbert, S. P., & Johnson, K. A. (1993) *Biochemistry* 32, 4677–4684.
- Gilbert, S. P., & Johnson, K. A. (1994) *Biochemistry* 33, 1951–1960.
- Gilbert, S. P., Moyer, M. L., & Johnson, K. A. (1998) *Biochemistry* 37, 792–799.
- Hackney, D. D. (1994a) *Proc. Natl. Acad. Sci. U.S.A.* 91, 6865–6869.
- Hackney, D. D. (1994b) *J. Biol. Chem.* 269, 16508–16511.
- Hackney, D. D. (1995a) *Biophys. J.* 68 Suppl. 267S.
- Hackney, D. D. (1995b) *Nature* 377, 448–450.
- Hiratsuka, T. (1983) *Biochim. Biophys. Acta* 742, 496–508.
- Howard, J., Hudspeth, A. J., & Vale, R. D. (1989) *Nature* 342, 154–158.
- Huang, T. G., & Hackney, D. D. (1994) *J. Biol. Chem.* 269, 16493–16501.
- Jiang, W., & Hackney, D. D. (1997) *J. Biol. Chem.* 272, 5616–5621.
- Jiang, W., Stock, M. F., Li, X., & Hackney, D. D. (1997) *J. Biol. Chem.* 272, 7626–7632.
- Kull, F. J., Sablin, E. P., Lau, R., Fletterick, R. J., & Vale, R. D. (1996) *Nature* 380, 550–555.
- Kuznetsov, S. A., Vaisberg, E. A., Shanina, N. A., Magretova, N. N., Chernyak, V. Y., & Gelfand, V. I. (1988) *EMBO J.* 7, 353–356.
- Lanzetta, P. A., Alvarez, L. J., Reinach, P. S., & Candia, O. A. (1979) *Anal. Biochem.* 100, 95–97.
- Lockhart, A., Crevel, I. M.-T. C., & Cross, R. A. (1995) *J. Mol. Biol.* 249, 763–771.
- Lowey, S., & Cohen, C. (1962) *J. Mol. Biol.* 4, 293–308.
- Lowry, O. H., Rosebrough, N. J., Farr, A. L., & Randall, R. J. (1951) *J. Biol. Chem.* 193, 265–275.
- Ma, Y. Z., & Taylor, E. W. (1995) *Biochemistry* 34, 13242–13251.
- Ma, Y. Z., & Taylor, E. W. (1997a) *J. Biol. Chem.* 272, 717–723.
- Ma, Y. Z., & Taylor, E. W. (1997b) *J. Biol. Chem.* 272, 724–730.
- Margossian, S. S., & Lowey, S. (1973) *J. Mol. Biol.* 74, 301–311.
- Moore, K. J. M., & Lohman, T. M. (1994) *Biochemistry* 33, 14550–14564.
- Moyer, M. L., Gilbert, S. P., & Johnson, K. A. (1996) *Biochemistry* 35, 6321–6329.

- Omoto, C. K., & Johnson, K. A. (1986) *Biochemistry* 25, 419–427.
- Rayment, I., Rypniewski, W. R., Schmidt-Base, K., Smith, R., Tomchick, D. R., Benning, M. M., D. A., Wesenberg Winkelmann, G., & Holden, H. M. (1993) *Science* 261, 50–58.
- Rosenfeld, S. S., Renner, B., Correia, J. J., Mayo, M. S., & Cheung, H. C. (1996) *J. Biol. Chem.* 271, 9473–9482.
- Schacterle, G. R., & Pollack, R. L. (1973) *Anal. Biochem.* 51, 654–655.
- Shelanski, M. L., Gaskin, F., & Cantor, C. R. (1973) *Proc. Natl. Acad. Sci. U.S.A.* 70, 765–768.
- Sloboda, R. D., Dentler, W. L., & Rosenbaum, J. L. (1976) *Biochemistry* 15, 4497–4505.
- Stewart, R. J., Thaler, J. P., & Goldstein, L. S. (1993) *Proc. Natl. Acad. Sci. U.S.A.* 90, 5209–5213.
- Vale, R. D., Funatsu, T., Pierce, D. W., Romberg, L., Harada, Y., & Yanagida, T. (1996) *Nature* 380, 451–453.
- Weeds, A. G., & Lowey, S. (1971) *J. Mol. Biol.* 61, 701–725.
- Woodward, S. K. A., Eccleston, J. F., & Geeves, M. A. (1991) *Biochemistry* 30, 422–430.
- Yang, J. T., Saxton, W. M., Stewart, R. J., Raff, E. C., & Goldstein, L. S. B. (1990) *Science* 249, 42–47.
- Zimmerle, C. J., and Frieden, C. (1989) *Biochem. J.* 258, 381–387.

BI9711184